Research Article | Vol. 6, No. 8 | 1 Aug 2016 | OPTICAL MATERIALS EXPRESS 2616

Optical Materials EXPRESS

Selenide sputtered films development for MIR environmental sensor

E. BAUDET,[1] A. GUTIERREZ-ARROYO,[2] P. NĚMEC,[3] L. BODIOU,[2] J. LEMAITRE,[2] O. DE SAGAZAN,[4] H. LHERMITTE,[4] E. RINNERT,[5] K. MICHEL,[6] B. BUREAU,[1] J. CHARRIER,[2] AND V. NAZABAL[1*]

[1]*Institut des Sciences Chimiques de Rennes, UMR-CNRS 6226, Equipe Verres et Céramiques, Université de Rennes 1, 35042 Rennes, France*
[2]*FOTON -UMR-CNRS 6082, ENSSAT BP80518, F-22305 Lannion Cedex, France*
[3]*Department of Graphic Arts and Photophysics, Faculty of Chemical Technology, University of Pardubice, Studentska 573, 53210 Pardubice, Czech Republic*
[4]*IETR, Université de Rennes 1, 35042 Rennes, France*
[5]*IFREMER, Laboratoire Détection, Capteurs et Mesures, Dpt. Recherches et Développements Technologiques, 29280 Plouzané, France*
[6]*BRGM, Direction Eau, Environnement et Ecotechnologies, Unité Bio-Géochimie Environnementale et Qualité de l'Eau, 45060, Orléans, France*
**virginie.nazabal@univ-rennes1.fr*

Abstract: A micro-sensor based on selenide glasses for evanescent wave detection in mid-infrared spectral range was designed and fabricated. Ge-Sb-Se thin films were successfully deposited by radio-frequency magnetron sputtering. In order to characterize them spectroscopic ellipsometry, atomic force microscopy and contact angle measurements were employed to study near and middle infrared refractive index, surface roughness and the wettability, respectively. Selenide sputtered films were micro-patterned by means of reactive ion etching with inductively coupled plasma process enabling single-mode propagation at a wavelength of 7.7 µm for a waveguide width between 8 and 12 µm. Finally, optical waveguide surface was functionalized by deposition of a hydrophobic polymer, which will permit detection of organic molecules in water. Thus, the optical transducer is a ridge waveguide composed by cladding and guiding Ge-Sb-Se sputtered layers exhibiting a tailored refractive index contrast and a polymer layer onto its surface ready for environmental detections in middle infrared.

OCIS codes: (130.3120) Integrated optics devices; (160.2750) Glass and other amorphous materials; (310.6860) Thin films, optical properties; (280.4788) Optical sensing and sensors.

References and links

1. B. Bureau, C. Boussard-Pledel, J. Troles, V. Nazabal, J. L. Adam, J. L. Doualan, A. Braud, P. Camy, P. Lucas, L. Brilland, L. Quetel, and H. Tariel, "Development of optical fibers for mid-infrared sensing: State of the art and recent achievements," in *Micro-Structured and Specialty Optical Fibres Iv*, K. Kalli, J. Kanka, and A. Mendez, eds. (2015).
2. B. Mizaikoff, "Waveguide-enhanced mid-infrared chem/bio sensors," Chem. Soc. Rev. **42**(22), 8683–8699 (2013).
3. R. Lu, W. W. Li, A. Katzir, Y. Raichlin, H. Q. Yu, and B. Mizaikoff, "Probing the secondary structure of bovine serum albumin during heat-induced denaturation using mid-infrared fiberoptic sensors," Analyst (Lond.) **140**(3), 765–770 (2015).
4. V. Singh, P. T. Lin, N. Patel, H. T. Lin, L. Li, Y. Zou, F. Deng, C. Y. Ni, J. J. Hu, J. Giammarco, A. P. Soliani, B. Zdyrko, I. Luzinov, S. Novak, J. Novak, P. Wachtel, S. Danto, J. D. Musgraves, K. Richardson, L. C. Kimerling, and A. M. Agarwal, "Mid-infrared materials and devices on a Si platform for optical sensing," Sci. Technol. Adv. Mater. **15**, 1 (2014).
5. F. Starecki, F. Charpentier, J. L. Doualan, L. Quetel, K. Michel, R. Chahal, J. Troles, B. Bureau, A. Braud, P. Camy, V. Moizan, and V. Nazabal, "Mid-IR optical sensor for CO_2 detection based on fluorescence absorbance of Dy^{3+}:$Ga_5Ge_{20}Sb_{10}S_{65}$ fibers," Sens. Actuators B Chem. **207**, 518–525 (2015).
6. N. Singh, D. D. Hudson, R. Wang, E. C. Mägi, D.-Y. Choi, C. Grillet, B. Luther-Davies, S. Madden, and B. J. Eggleton, "Positive and negative phototunability of chalcogenide (AMTIR-1) microdisk resonator," Opt. Express **23**(7), 8681–8686 (2015).
7. P. Ma, D.-Y. Choi, Y. Yu, Z. Yang, K. Vu, T. Nguyen, A. Mitchell, B. Luther-Davies, and S. Madden, "High Q factor chalcogenide ring resonators for cavity-enhanced MIR spectroscopic sensing," Opt. Express **23**(15), 19969–19979 (2015).
8. J. Charrier, M.-L. Brandily, H. Lhermite, K. Michel, B. Bureau, F. Verger, and V. Nazabal, "Evanescent wave optical micro-sensor based on chalcogenide glass," Sens. Actuators B Chem. **173**, 468–476 (2012).

#264299 http://dx.doi.org/10.1364/OME.6.002616
Journal © 2016 Received 29 Apr 2016; revised 28 Jun 2016; accepted 28 Jun 2016; published 19 Jul 2016

Optical Materials EXPRESS

9. Y. Chen, H. Lin, J. Hu, and M. Li, "Heterogeneously integrated silicon photonics for the mid-infrared and spectroscopic sensing," ACS Nano **8**(7), 6955–6961 (2014).
10. Y.-C. Chang, P. Wägli, V. Paeder, A. Homsy, L. Hvozdara, P. van der Wal, J. Di Francesco, N. F. de Rooij, and H. Peter Herzig, "Cocaine detection by a mid-infrared waveguide integrated with a microfluidic chip," Lab Chip **12**(17), 3020–3023 (2012).
11. J. Hu, "Ultra-sensitive chemical vapor detection using micro-cavity photothermal spectroscopy," Opt. Express **18**(21), 22174–22186 (2010).
12. D. McMullin, B. Mizaikoff, and R. Krska, "Advancements in IR spectroscopic approaches for the determination of fungal derived contaminations in food crops," Anal. Bioanal. Chem. **407**(3), 653–660 (2015).
13. Z. Han, P. Lin, V. Singh, L. Kimerling, J. Hu, K. Richardson, A. Agarwal, and D. T. H. Tan, "On-chip mid-infrared gas detection using chalcogenide glass waveguide," Appl. Phys. Lett. **108**, 141106 (2016).
14. C. Vigreux, E. Barthélémy, L. Bastard, J. E. Broquin, M. Barillot, S. Ménard, G. Parent, and A. Pradel, "Realization of single-mode telluride rib waveguides for mid-IR applications between 10 and 20 μm," Opt. Lett. **36**(15), 2922–2924 (2011).
15. P. Němec, M. Olivier, E. Baudet, A. Kalendová, P. Benda, and V. Nazabal, "Optical properties of (GeSe2)100−x(Sb2Se3)x glasses in near- and middle-infrared spectral regions," Mater. Res. Bull. **51**, 176–179 (2014).
16. M. Olivier, J. C. Tchahame, P. Nemec, M. Chauvet, V. Besse, C. Cassagne, G. Boudebs, G. Renversez, R. Boidin, E. Baudet, and V. Nazabal, "Structure, nonlinear properties, and photosensitivity of $(GeSe_2)_{100-x}(Sb_2Se_3)_x$ glasses," Opt. Mater. Express **4**(3), 525–540 (2014).
17. D. D. Hudson, M. Baudisch, D. Werdehausen, B. J. Eggleton, and J. Biegert, "1.9 octave supercontinuum generation in a As_2S_3 step-index fiber driven by mid-IR OPCPA," Opt. Lett. **39**(19), 5752–5755 (2014).
18. U. Møller, Y. Yu, I. Kubat, C. R. Petersen, X. Gai, L. Brilland, D. Méchin, C. Caillaud, J. Troles, B. Luther-Davies, and O. Bang, "Multi-milliwatt mid-infrared supercontinuum generation in a suspended core chalcogenide fiber," Opt. Express **23**(3), 3282–3291 (2015).
19. B. J. Eggleton, B. Luther-Davies, and K. Richardson, "Chalcogenide photonics," Nat. Photonics **5**, 141–148 (2011).
20. C. C. Huang, B. Gholipour, J. Y. Ou, K. Knight, and D. W. Hewak, "Electrical phase change of CVD-grown Ge-Sb-Te thin-film device," Electron. Lett. **47**, 288 (2011).
21. C. C. Huang, C. C. Wu, K. Knight, and D. W. Hewak, "Optical properties of CVD grown amorphous Ge-Sb-S thin films," J. Non-Cryst. Solids **356**(4-5), 281–285 (2010).
22. M. Frumar, H. Ticha, M. Vlcek, J. Klikorka, and L. Tichy, "Photostructural changes in some ternary Ge-Sb-S chalcogenide layers," Czech. J. Phys. **31**(4), 441–446 (1981).
23. M. Frumar, B. Frumarová, T. Wágner, P. Němec: Photo-induced phenomena in amorphous and glassy chalcogenides, in: *Photo-induced Metastability in Amorphous Semiconductor*s (ed. A.V.Kolobov), (Wiley-VCH, Weinheim, 2003) 23-44.
24. J. D. Musgraves, N. Carlie, J. Hu, L. Petit, A. Agarwal, L. C. Kimerling, and K. A. Richardson, "Comparison of the optical, thermal and structural properties of Ge-Sb-S thin films deposited using thermal evaporation and pulsed laser deposition techniques," Acta Mater. **59**(12), 5032–5039 (2011).
25. K. Petkov and B. Dinev, "Photoinduced changes in the optical-properties of amorphous As-Ge-S thin-films," J. Mater. Sci. **29**(2), 468–472 (1994).
26. K. E. Youden, T. Grevatt, R. W. Eason, H. N. Rutt, R. S. Deol, and G. Wylangowski, "Pulsed-Laser Deposition of Ga-La-S Chalcogenide Glass Thin-Film Optical Wave-Guides," Appl. Phys. Lett. **63**(12), 1601–1603 (1993).
27. P. Nemec, M. Frumar, B. Frumarova, M. Jelinek, J. Lancok, and J. Jedelsky, "Pulsed laser deposition of pure and praseodymium-doped Ge-Ga-Se amorphous chalcogenide films," Opt. Mater. **15**(3), 191–197 (2000).
28. A. Zakery, "Low loss waveguides in pulsed laser deposited arsenic sulfide chalcogenide films," J. Phys. D Appl. Phys. **35**(22), 2909–2913 (2002).
29. S. Ramachandran and S. G. Bishop, "Excitation of Er3+ emission by host glass absorption in sputtered films of Er-doped Ge10As40Se25S25 glass," Appl. Phys. Lett. **73**(22), 3196 (1998).
30. J. Charrier, M. L. Anne, H. Lhermite, V. Nazabal, J. P. Guin, T. Jouan, F. Henrio, D. Bosc, and J. L. Adam, "Sulphide $Ga_xGe_{25-x}Sb_{10}S_{65\ (x=0,\ 5)}$ sputtered films: fabrication and optical characterisation of planar and rib optical waveguides," J. Appl. Phys. **104**(7), 073110 (2008).
31. R. Siebert, and J. Muller, "Infrared integrated optical evanescent field sensor for gas analysis Part I: System design," Sensors and Actuators A-Physical **119**, 138–149 (2005).
32. J. Charrier, M. L. Brandily, H. Lhermite, K. Michel, B. Bureau, F. Verger, and V. Nazabal, "Evanescent wave optical micro-sensor based on chalcogenide glass," Sens. Actuators B Chem. **173**, 468–476 (2012).
33. K. Flavin, H. Hughes, V. Dobbyn, P. Kirwan, K. Murphy, H. Steiner, B. Mizaikoff, and P. McLoughlin, "A comparison of polymeric materials as pre-concentrating media for use with ATR/FTIR sensing," Int. J. Environ. Anal. Chem. **86**(6), 401–415 (2006).
34. B. Pejcic, L. Boyd, M. Myers, A. Ross, Y. Raichlin, A. Katzir, R. Lu, and B. Mizaikoff, "Direct quantification of aromatic hydrocarbons in geochemical fluids with a mid-infrared attenuated total reflection sensor," Org. Geochem. **55**, 63–71 (2013).
35. G. E. Jellison and F. A. Modine, "Parameterization of the optical functions of amorphous materials in the interband region," Appl. Phys. Lett. **69**, 2137–2137 (1996).
36. A. S. Ferlauto, G. M. Ferreira, J. M. Pearce, C. R. Wronski, R. W. Collins, X. M. Deng, and G. Ganguly, "Analytical model for the optical functions of amorphous semiconductors from the near-infrared to ultraviolet: Applications in thin film photovoltaics," J. Appl. Phys. **92**(5), 2424–2436 (2002).

Optical Materials EXPRESS

37. P. Nemec, V. Nazabal, and M. Frumar, "Photoinduced phenomena in amorphous As_4Se_3 pulsed laser deposited thin films studied by spectroscopic ellipsometry," J. Appl. Phys. **106**, 023509 (2009).
38. P. Němec, S. Zhang, V. Nazabal, K. Fedus, G. Boudebs, A. Moreac, M. Cathelinaud, and X. H. Zhang, "Photo-stability of pulsed laser deposited $Ge_xAs_ySe_{100-x-y}$ amorphous thin films," Opt. Express **18**(22), 22944–22957 (2010).
39. D. K. Owens, and R. C. Wendt, "Estimation of surface free energy of polymers," J. Appl. Polym. Sci. **13**, 1741 (1969).
40. J. Charrier, M. L. Anne, H. Lhermite, V. Nazabal, J. P. Guin, F. Charpentier, T. Jouan, F. Henrio, D. Bosc, and J. L. Adam, "Sulphide $Ga_{(x)}Ge_{(25-x)}Sb_{(10)}S_{(65(x=0,5))}$ sputtered films: Fabrication and optical characterizations of planar and rib optical waveguides," J. Appl. Phys. **104**(7), 073110 (2008).
41. M. Olivier, P. Nemec, G. Boudebs, R. Boidin, C. Focsa, and V. Nazabal, "Photosensitivity of pulsed laser deposited Ge-Sb-Se thin films," Opt. Mater. Express **5**(4), 781–793 (2015).
42. F. Verger, V. Nazabal, F. Colas, P. Nemec, C. Cardinaud, E. Baudet, R. Chahal, E. Rinnert, K. Boukerma, I. Peron, S. Deputier, M. Guilloux-Viry, J. P. Guin, H. Lhermite, A. Moreac, C. Compere, and B. Bureau, "RF sputtered amorphous chalcogenide thin films for surface enhanced infrared absorption spectroscopy," Opt. Mater. Express **3**(12), 2112–2131 (2013).
43. J. Amalric and J. Marchand-Brynaert, "Surface modification of amorphous substrates by disulfide derivatives: A photo-assisted route to direct functionalization of chalcogenide glasses," Surf. Sci. **605**(23-24), 2006–2016 (2011).
44. P. Lucas, M. A. Solis, D. Le Coq, C. Juncker, M. R. Riley, J. Collier, D. E. Boesewetter, C. Boussard-Pledel, and B. Bureau, "Infrared biosensors using hydrophobic chalcogenide fibers sensitized with live cells," Sens. Actuators B Chem. **119**(2), 355–362 (2006).
45. M. Karlowatz, M. Kraft, and B. Mizaikoff, "Simultaneous quantitative determination of benzene, toluene, and xylenes in water using mid-infrared evanescent field spectroscopy," Anal. Chem. **76**(9), 2643–2648 (2004).
46. J. T. Robinson, K. Preston, O. Painter, and M. Lipson, "First-principle derivation of gain in high-index-contrast waveguides," Opt. Express **16**(21), 16659–16669 (2008).
47. D. Y. Choi, S. Maden, A. Rode, R. P. Wang, and B. Luther-Davies, "Plasma etching of $AS_{(2)}S_{(3)}$ films for optical waveguides," J. Non-Cryst. Solids **354**(27), 3179–3183 (2008).
48. J. Chiles, M. Malinowski, A. Rao, S. Novak, K. Richardson, and S. Fathpour, "Low-loss, submicron chalcogenide integrated photonics with chlorine plasma etching," Appl. Phys. Lett. **106**(11), 111110 (2015).
49. Y. Ruan, W. Li, R. Jarvis, N. Madsen, A. Rode, and B. Luther-Davies, "Fabrication and characterization of low loss rib chalcogenide waveguides made by dry etching," Opt. Express **12**(21), 5140–5145 (2004).
50. D. Y. Choi, S. Madden, A. Rode, R. Wang, and B. Luther-Davies, "Fabrication of low loss $Ge_{33}As_{12}Se_{55}$ (AMTIR-1) planar waveguides," Appl. Phys. Lett. **91**(1), 011115 (2007).
51. B. Pejcic, M. Myers, and A. Ross, "Mid-infrared sensing of organic pollutants in aqueous environments," Sensors (Basel) **9**(8), 6232–6253 (2009).
52. E. Baudet, K. Michel, J. Moreau, P. Němec, B. Bureau, V. Nazabal, and E. Rinnert, "MIR attenuated total reflection sensor for the detection of aromatic hydrocarbons in water," submitted (2016).

1. Introduction

Pollution of groundwater or seawater is actually an ecological issue which requires monitoring with high stability, selectivity, large detection range, compactness and short response time. As a result, the development of environmental sensors for in situ measurements is a great challenge for the detection of pollutant molecules in water. The middle infrared (MIR) spectroscopy can answer these prospects as its spectral range covering 2.5 – 25 μm contains the molecular vibrational absorption bands related to various molecules (mainly organic compounds). Consequently, the MIR spectroscopy is hugely exploited by means of classical tools for analyzing food, drinks, toxic agents, explosives, greenhouse gases, air and water pollutants, pharmaceutical systems, proteins, cells, polymers and frequently used in Chemistry, Manufacturing and Control (CMC) process. This is why the potential of MIR photonics implementation is considerable and recent advances in the development of optical chemical and bio-sensors were made in this specific range of wavelength [1–6].

Environmental sensors based on evanescent field detection are sensitive to the optical changes induced by the analyte, such as its absorption. The evanescent field, i.e. a fraction of the guided light outside of the waveguide, can probe the external medium surrounding the waveguide. The amplitude of the evanescent field in the external medium (gas or liquid) decays exponentially with the distance from the waveguide surface. Compare to fiber optical sensor, the chip-scale waveguides benefit from device miniaturization, low-cost production with ability for mass fabrication, better mechanical strength and low sensitivity to environmental requirements. However, integrated devices' development is limited by the availability of efficient, low cost and silicon compatible

Optical Materials EXPRESS

materials for MIR sources and detectors, low optical losses or unsatisfactory IR transmittance of the used materials. That is why only a few reports on the development of miniaturized optical (bio)-chemical sensor dedicated to MIR are available, especially in the range of 6-12 µm [4, 7–13].

Chalcogenide glasses can be considered as appropriate materials for sensing applications because they have specific optical characteristics making them easy-to-use for integrated MIR optical devices. Thanks to their wide transparency in the infrared range [1, 14] and high linear and nonlinear refractive index [15–19] chalcogenide glasses are commonly used for photonics devices. To fabricate MIR sensor platform, it is required to pattern chalcogenide thin films and diverse methods can be used for chalcogenide thin films' deposition such as chemical vapor deposition [20, 21], thermal evaporation [22–25], pulsed laser deposition [26–28] or RF magnetron sputtering [29, 30].

In this paper, we report the fabrication of selenide sputtered films and the development of chalcogenide waveguides dedicated to MIR spectroscopy. The RF magnetron sputtering method is probably not the most anticipated deposition method for MIR wavelengths requiring significant thicknesses even if the optical quality of sputtered thin films are known to be of high-quality compare to evaporation or pulsed laser deposition methods; with surely low roughness and dense films, defect-free and well-adhered interface, interesting layer homogeneity and uniformity. With such a material challenge, synthesis and characterization were performed in order to propose sputtered amorphous chalcogenide thick film with suitable morphology, topography, composition control and appropriate optogeometric design for MIR sensor fabrication. In first stage, the choice of chalcogenide glass composition, the chalcogenide films synthesis through sputtering, the patterning of the films by means of reactive ion etching and the physical/chemical characteristics will be described. Then, the injection of Quantum Cascade Laser (QCL) source emitting at 7.7 µm into MIR waveguides made of chalcogenide core and buffer layers deposited on silicon substrates will be studied to demonstrate their potential use as a MIR sensor. Finally, the compatibility of functionalization, devoted to molecules detection in water, between a Ge-Sb-Se selenide waveguide surface and a specific hydrophobic polymer will be presented.

2. Materials and experimental methods

2.1. Synthesis of Ge-Sb-Se glass targets

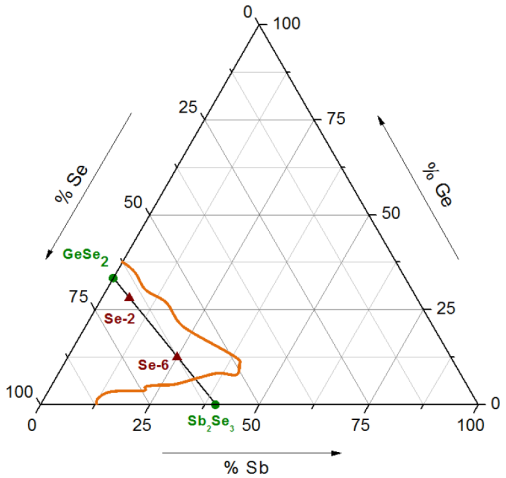

Fig. 1. Ge-Sb-Se ternary diagram with glass-forming region (orange line) showing studied compositions: $(GeSe_2)_{90}(Sb_2Se_3)_{10}$(Se-2) and $(GeSe_2)_{50}(Sb_2Se_3)_{50}$(Se-6) [16].

Chalcogenide glass targets with $Ge_{28.1}Sb_{6.3}Se_{65.6}$ (i.e. $(GeSe_2)_{90}(Sb_2Se_3)_{10}$) and $Ge_{12.5}Sb_{25}Se_{62.5}$ (i.e. $(GeSe_2)_{50}(Sb_2Se_3)_{50}$) nominal composition (Fig. 1) were prepared using the conventional melting and quenching method. The glasses were synthesized

Optical Materials EXPRESS

using high purity (5N) commercial elements (Ge, Sb and Se). Selenium was pre-purified by static distillation. The elements were weighted and introduced in appropriate amounts into a silica ampoule with a diameter of 50 mm. After the evacuation and sealing, the batches were melted in a rocking furnace at 850 °C during 12 hours, quenched in water and annealed at a temperature close to their glass transition temperature, i.e. ~330 and ~205 °C for $Ge_{28.1}Sb_{6.3}Se_{65.6}$ and $Ge_{12.5}Sb_{25}Se_{62.5}$ glasses, respectively. Chalcogenide glass targets were obtained after cutting and polishing of the glass rods.

2.2. Thin films and MIR guiding structure deposition by RF magnetron sputtering

Chalcogenide glass targets ($Ge_{28.1}Sb_{6.3}Se_{65.6}$ and $Ge_{12.5}Sb_{25}Se_{62.5}$) were used for thin films deposition employing RF magnetron sputtering. The deposition was carried out under Ar pressure (1.10^{-2} mbar) using silicon substrates. Considering the insulator character of the chalcogenide targets, the sputtering was performed at low RF working power: 20 and 10 W for $Ge_{28.1}Sb_{6.3}Se_{65.6}$ and $Ge_{12.5}Sb_{25}Se_{62.5}$ targets, respectively. Appropriate deposition time was determined to obtain films' thicknesses of 5 and 1.7 µm for $Ge_{28.1}Sb_{6.3}Se_{65.6}$ and $Ge_{12.5}Sb_{25}Se_{62.5}$ composition, respectively. MIR guiding structure is composed of two layers; the first one is a $Ge_{28.1}Sb_{6.3}Se_{65.6}$ film with a thickness of 5 µm (cladding layer) and the second is a $Ge_{12.5}Sb_{25}Se_{62.5}$ film with a thickness of 1.7 µm (guiding layer). MIR waveguide was elaborated using deposition parameters mentioned above. An off-axis substrates rotation was operated during the deposition process and the substrates were placed at the target to substrate distance of 5 cm.

2.3. Development of Ge-Sb-Se selenide waveguide

Applying the refractive indices of single Ge-Sb-Se selenide layers knowledge, simulations to determine the design of optical waveguide working in MIR (at 7.7 µm) were performed. The MIR structure consists of a superstrate (hydrophobic polymer), $Ge_{12.5}Sb_{25}Se_{62.5}$ guiding layer and $Ge_{28.1}Sb_{6.3}Se_{65.6}$ cladding layer, deposited on silicon substrate. The thicknesses of both chalcogenide layers and the width of the waveguide were established in order to obtain singlemode propagation at 7.7 µm and a maximum evanescent power factor η [31, 32]. The evanescent power corresponds to the part of the electromagnetic field which is not confined in the guiding layer ($Ge_{12.5}Sb_{25}Se_{62.5}$) and which consequently interacts with the analyte in the liquid which is in contact with the waveguide surface. A 5 µm-thick $Ge_{28.1}Sb_{6.3}Se_{65.6}$ confinement layer was found to be sufficient to avoid radiation losses through the substrate. Thickness of $Ge_{12.5}Sb_{25}Se_{62.5}$ guiding layer between 1.5 and 2 µm allows obtaining single-mode propagation at a wavelength of 7.7 µm for a waveguide width between 8 and 12 µm and for TM polarization by using FIMMWAVE mode solvers. A classical i-line photolithography process (MJB4 Suss Microtech mask aligner) with S1805 positive photoresist was used before dry etching. Guiding $Ge_{12.5}Sb_{25}Se_{62.5}$ layer was then etched by a reactive ion etching at low pressure (Corial 200IL) with inductively coupled plasma (RIE-ICP) exploiting CHF_3 gas.

2.4. Functionalization of chalcogenide waveguide

To use chalcogenide waveguide as a sensor for the detection of pollutants in water, a hydrophobic polymer was deposited onto the guiding layer to extract molecules from the contaminated water and to avoid its high absorbance in this spectral range. In detail, a thin polymer film was coated onto the chalcogenide waveguide by placing 500 µL of a xylene solution that contained polyisobutylene (PIB, Sigma-Aldrich) with a 1% (w/v) concentration. The PIB was deposited by spin coating (Spinner Laurell WS-400B-6NPP-Lite) at speed of rotation of 500 rpm. The appropriate superstrate thickness is estimated according to the penetration depth d_p of the evanescent field (Eq. (1):

$$d_p = \frac{\lambda}{2\pi n_1 \left[\sin^2\theta - \left(n_2 / n_1 \right)^2 \right]^{1/2}} \quad (1)$$

Optical Materials EXPRESS

where λ is the wavelength of the incident light, n_1 and n_2 are refractive indices of waveguide and superstrate respectively and θ is the angle of incidence. It is recommended that the polymer thickness should be roughly three times of the penetration depth to ensure sufficient detection sensitivity and short response time [33, 34].

2.5. Targets, films and MIR structure characterization

The chemical composition of $Ge_{28.1}Sb_{6.3}Se_{65.6}$ and $Ge_{12.5}Sb_{25}Se_{62.5}$ targets and films was measured using a scanning electron microscope (SEM) with an energy-dispersive X-ray analyzer (EDS, JSM 6400-OXFORD Link INCA). The SEM technique was also applied to observe thin films and MIR structure morphology using a field emission gun SEM (JSM 6301F).

Linear refractive indices of glasses, thin films and each layer of MIR guiding structure were obtained from the analysis of variable angle spectroscopic ellipsometry (VASE) data measured using two ellipsometers: a rotating analyzer ellipsometer measuring in UV-Vis-NIR (300-2300 nm) and a rotating compensator ellipsometer working in NIR-MIR (1.7-30 µm) (J.A. Woollam Co., Inc., Lincoln, NE, USA). The VASE data were recorded at three angles of incidence (65°, 70° and 75° for thin films and MIR structure, 50°, 60° and 70° for bulk glasses). The resolution of UV-Vis-NIR ellipsometer of 20, 10 or 5 nm was selected. NIR-MIR ellipsometer resolution was set to 2, 8 or 16 cm^{-1}. The resolution used for individual measurement was selected in accordance with expected thickness of MIR structure, $Ge_{28.1}Sb_{6.3}Se_{65.6}$ and $Ge_{12.5}Sb_{25}Se_{62.5}$ thin films. The Cody-Lorentz model [35, 36] was used to analyze VASE data of targets and films; this model is appropriate for the description of amorphous chalcogenides optical function [37, 38]. The Sellmeier model was used for IR structure analysis. Thicknesses and optical band-gap values were also deduced from VASE data, where possible.

Finally, roughness of thin films was studied by atomic force microscopy (AFM, Ntegra Prima, NT-MDT). Tapping mode imaging was used on 2 µm x 2 µm area.

2.6. Contact angle measurement – Surface tension

Contact angle measurements were performed on $Ge_{28.1}Sb_{6.3}Se_{65.6}$ and $Ge_{12.5}Sb_{25}Se_{62.5}$ thin films. A drop of liquid was deposited on the surface of the sample and the tangent at the base of the drop was recorded. Contact angle was calculated via image analysis. The measurement was realized with five different liquids (water, glycerol, ethylene glycol, formamide and diiodomethane) with an acquisition time of 20 seconds. In order to determine surface tension of thin films, Owens-Wendt [39] method was used.

2.7. Optical characterization of ridge waveguides

Optical loss measurement was executed at 1.55 µm using surface imaging method [40] within the IR guiding structure. The single-mode laser light was singled-mode fiber-coupled into the waveguide. The intensity of the scattered light was recorded with a camera placed above the sample. Transverse scanning along the direction of light propagation enabled us to obtain the two-dimensional light intensity distribution of the waveguide modes. The longitudinal variation was obtained by integrating the data along transverse lines. Optical characterizations at 7.7 µm (1290 cm^{-1}) were performed by coupling a QCL (Alpes Lasers) into the ridge waveguides through a ZnSe microscope objective (Innovation Photonics) and imaging the output facet on a microbolometer-based focal plane array (FPA, Optris PI400) using a second ZnSe microscope objective.

3. Results and discussion

3.1. Ge-Sb-Se targets and films characterization

The choice of the composition of the films was pondered by considering that for the development of environmental sensor or sensor devoted to the medical field, it is better to avoid the using of layers containing arsenic, which is toxic in its elemental form. Arsenic-containing compositions could be unacceptable for end-users especially for continuous water analysis even if they have interesting properties and are often studied. Advantages of selenide-based chalcogenide glasses and thin films in comparison with sulfide ones for

Optical Materials EXPRESS

sensor development are broader transmission window in infrared spectral region, larger glass-forming system (Ge-Sb-Se vs. Ge-Sb-S system) allowing tailoring of physical parameters of interest in broad ranges. Also, the presence of antimony in amorphous chalcogenides is known to reduce photosensitivity of both, the bulk glasses and thin films which can induce formation of oxide crystallites on layer surface as classically observed for As_2Se_3. The selection of the two distinct compositions from Ge-Sb-Se system studied in this work is based on our previous experience with this glassy system [15, 16, 41, 42], permitting desired refractive index contrast between individual thin films of the fabricated structures.

The chemical composition of $Ge_{28.1}Sb_{6.3}Se_{65.6}$ and $Ge_{12.5}Sb_{25}Se_{62.5}$ bulk targets and sputtered thin films is presented in Table 1. The presented data show that the chemical composition of chalcogenide targets is in good agreement with the theoretical composition considering EDS measurement uncertainty of about ± 1 at. %. The chemical composition of $Ge_{28.1}Sb_{6.3}Se_{65.6}$ and $Ge_{12.5}Sb_{25}Se_{62.5}$ sputtered thin films deposited under 1.10^{-2} mbar Ar pressure are relatively close to the nominal composition of target. However, the films present an excess in germanium, 3.9 and 2.2 at. %. In the case of selenium, a deficit can be noted for both compositions: 3.7 and 2.2 at. % for $Ge_{28.1}Sb_{6.3}Se_{65.6}$ and $Ge_{12.5}Sb_{25}Se_{62.5}$ sputtered films, respectively. At last, a slight variation of antimony can be observed for $Ge_{28.1}Sb_{6.3}Se_{65.6}$ thin films (0.2 at. %) and no variation between target and sputtered film is observed for $Ge_{12.5}Sb_{25}Se_{62.5}$ composition. Compositional differences between the targets and sputtered thin films can be explained by different sputtering yield of each element of the target. In fact, high sputtering yield of chalcogen element leads to a Ge-Sb-Se target impoverished in Se and consequently sputtered thin film present some deficit in selenium content. Due to low atomic mass of germanium (compared to antimony), Ge is ejected easily from the target during sputtering process leading to an excess of the element in the films. Finally, antimony is a heavy element with high sputtering yield which results in (almost) no difference between the composition of the target and sputtered thin films.

Table 1 presents also refractive index values in NIR (1.55 µm) and MIR (6.3 and 7.7 µm) extracted from VASE data of the targets and corresponding RF sputtered thin films. The values of refractive index in MIR given in Table 1 were used for the simulation of optical waveguide design.

Table 1. Chemical composition (± 1 at.%) of bulk targets and sputtered thin films estimated by EDS. Refractive index in NIR and MIR (± 0.01) extracted from VASE data of bulk targets and sputtered $Ge_{28.1}Sb_{6.3}Se_{65.6}$ and $Ge_{12.5}Sb_{25}Se_{62.5}$ thin films. Surface RMS roughness (± 0.01 nm) of fabricated thin films obtained by AFM.

	$Ge_{28.1}Sb_{6.3}Se_{65.6}$		$Ge_{12.5}Sb_{25}Se_{62.5}$	
Chemical composition	**Target**	**Film**	**Target**	**Film**
Ge	27.6	31.5	12.6	14.8
Sb	6.0	5.8	24.5	24.5
Se	66.4	62.7	62.9	60.7
Refractive Index	**Target**	**Film**	**Target**	**Film**
1.55 µm	2.47	2.49	2.89	2.84
6.3 µm	2.43	2.45	2.82	2.78
7.7 µm	2.42	2.44	2.81	2.77
Roughness	-	**Film**	-	**Film**
RMS (nm)	-	0.44	-	0.78

The surface of RF sputtered thin films was observed by AFM and SEM (Fig. 2). Adequately low surface RMS roughness, that is lower than 1 nm, is observed (Table 1): 0.44 and 0.78 nm for $Ge_{28.1}Sb_{6.3}Se_{65.6}$ (thickness of 5 µm) and $Ge_{12.5}Sb_{25}Se_{62.5}$ thin films (thickness of 1.7 µm), respectively, which is appropriate for the light propagation in the optical waveguide.

Optical Materials EXPRESS

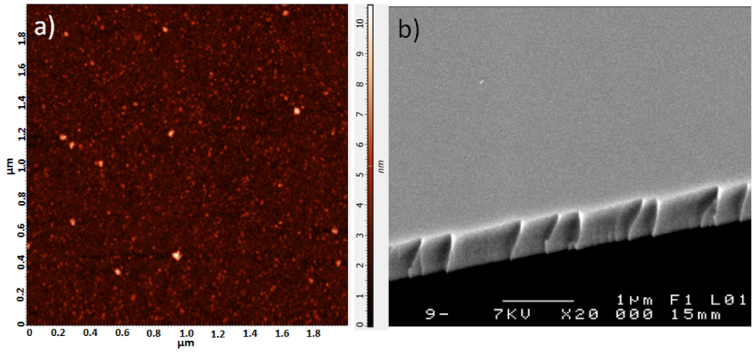

Fig. 2. (a) AFM image of surface and Fig. 2(b) SEM image of top surface and cross-section of $Ge_{12.5}Sb_{25}Se_{62.5}$ RF sputtered thin film.

3.2. Contact angle studies

Surface energy determination is very important when a material is developed for the detection in polluted water. Here, surface energy is calculated from contact angle measurements using Owens-Wendt approach. Table 2 presents contact angle θ measured between $Ge_{28.1}Sb_{6.3}Se_{65.6}$ or $Ge_{12.5}Sb_{25}Se_{62.5}$ thin films and different liquids (Fig. 3a). Contact angles of $Ge_{28.1}Sb_{6.3}Se_{65.6}$ and $Ge_{12.5}Sb_{25}Se_{62.5}$ thin films are comparable for both compositions, lower than 90° and tend to increase with surface tension of the liquid. These results are in agreement with contact angle measurement carried out between water and chalcogenide glasses [43] and fibers [44]. In order to study wetting behavior of thin films, Owens-Wendt method was used, allowing analysis of polar (γ^p) and dispersive (γ^d) components of total (γ_S) material surface energy (Fig. 3b). Surface energy is given by the evaluation of the slope a and the intercept b: $a^2 = \gamma_S{}^p$ and $b^2 = \gamma_S{}^d$.

Table 2. Contact angle and surface tension data obtained for $Ge_{28.1}Sb_{6.3}Se_{65.6}$ and $Ge_{12.5}Sb_{25}Se_{62.5}$ thin films.

Liquid	Contact angle θ		Surface tension ($mN.m^{-1}$)		
	$Ge_{28.1}Sb_{6.3}Se_{65.6}$	$Ge_{12.5}Sb_{25}Se_{62.5}$	$\gamma_L{}^d$	$\gamma_L{}^p$	γ_L
Water	78° ± 2°	73° ± 4°	21.8	51.0	72.8
Glycerol	62° ± 1°	58° ± 2°	34.0	30.0	64.0
Ethylene Glycol	48° ± 1°	46.1 ± 0.9°	29.3	19.0	48.3
Formamide	62° ± 1°	43.9° ± 0.6°	39.5	18.7	58.2
Diiodomethane	32° ± 3°	31.4° ± 0.9°	50.8	0	50.8

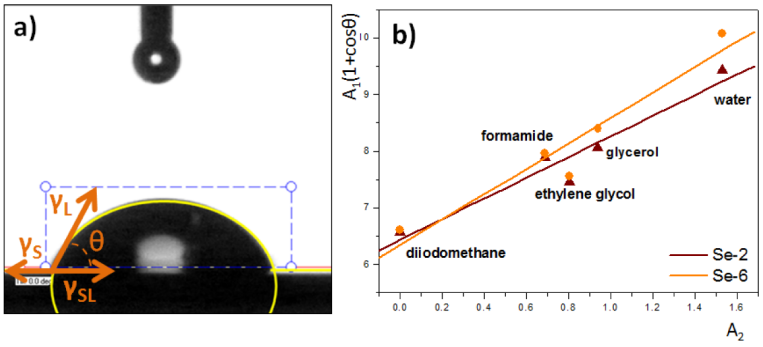

Fig. 3. (a) Image of contact angle measurement between water drop and $Ge_{28.1}Sb_{6.3}Se_{65.6}$ thin film. Contact angle θ is defined geometrically as the angle formed at the three phases boundary where liquid, gas and solid intersect and described by Young equation $\gamma_S = \gamma_{SL} + \gamma_L \cos\theta$. Figure 3(b) Surface energy of chalcogenide thin films within Owens-Wendt approach using five liquids with A1 = $\frac{\gamma_L}{2\sqrt{\gamma_L^d}}$ and A2 = $\frac{\sqrt{\gamma_L^p}}{\sqrt{\gamma_L^d}}$.

Optical Materials EXPRESS

Surface energy is approximately the same for both compositions (~46 $mN.m^{-1}$) indicating their similar wettability. Furthermore, it can be seen that polar component of chalcogenide thin films has very low value (~1 $mN.m^{-1}$). The hydrophobic thin film surface behavior can be explained through the presence of covalent bonds in the amorphous network. All three elements are neighbors within the periodic table having close electronegativities (Ge: 2.01, Sb: 2.05, Se: 2.55), consequently Ge-Sb-Se glasses are described as an amorphous network formed by strongly covalent bonds. As a result, thin films surface is devoid of polar sites favorable to hydrogen bonding with water molecules. Depicted hydrophobic behavior of Ge-Sb-Se films will contribute to limit the water absorption signal in this spectral range and obtaining better sensitivity for detection of pollutant molecules. However, notwithstanding this behavior, it is essential to use a hydrophobic material on waveguide surface to extract molecules to be detected from the water. Polymeric materials are commonly used for this purpose [33, 34, 45].

3.3. Simulation of optical waveguide

From the MIR refractive index data of the RF sputtered thin films, simulations based on the effective index method were performed to determine the geometrical parameters of the optical waveguide. In first approach, the coating layer as susperstrate was not considered in the simulation of this paper. Figure 4 presents the limits of single-mode propagation as a function of the width and the height of the guiding $Ge_{12.5}Sb_{25}Se_{62.5}$ layer. The effective index of the guided mode is between that of the guiding layer and of the cladding layer. Based on these limitations, evanescent power factor η of the fundamental mode as a function of w and h was calculated in the same figure by taking into account the high-index-contrast structure [46]. Thus, values of evanescent power factor η in MIR (λ = 7.7 µm) increase when h decreases, as Charrier *et al.* demonstrated for chalcogenide waveguide in near-IR (λ = 1.55 µm) [8]. A 1.7 µm thickness and a 10 µm width of the $Ge_{12.5}Sb_{25}Se_{62.5}$ guiding layer provided a good compromise regarding the evanescent power factor for the fundamental mode (η = 6%). With respect to the cladding layer ($Ge_{28.1}Sb_{6.3}Se_{65.6}$), the thickness was fixed at 5 µm to avoid light leak to the silicon substrate.

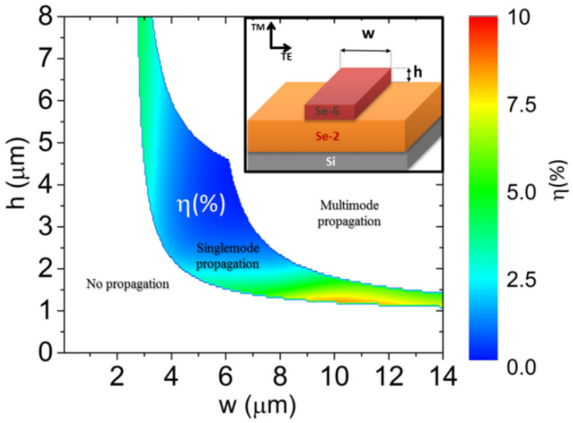

Fig. 4. The colored area as function of the dimensions w and h of the guiding layer defines the area where the effective index of the guided mode is between that of the guiding layer and the cladding layer. This colorful area also represents the evolution of the power factor evanescent 7.7 um (inset illustrates scheme of simulated ridge waveguide).

3.4. MIR structure and optical waveguide

MIR guiding structure, composed of the $Ge_{28.1}Sb_{6.3}Se_{65.6}$ cladding layer and the $Ge_{12.5}Sb_{25}Se_{62.5}$ guiding layer (Fig. 5(a)) was studied by VASE in order to control thickness of each layer and refractive indices in MIR. Firstly, thickness of guiding layer is close to those expected by simulations, i.e. 1.747 µm. In the case of the cladding layer,

Optical Materials EXPRESS

thickness is higher than intended thickness (5.467 µm) which leaves a supplementary margin to avoid light leak to the substrate. Figure 5(b) presents the dispersion curves of refractive indices of the guiding and cladding layers of the IR structure which are compared to single $Ge_{28.1}Sb_{6.3}Se_{65.6}$ and $Ge_{12.5}Sb_{25}Se_{62.5}$ thin films. A good agreement between single thin films and layers of MIR structure is obtained: for the cladding layer, refractive index at 6.3 and 7.7 µm is ~2.45; for the guiding layer, refractive indices are 2.77 and 2.76 respectively. The slight differences from refractive indices of $Ge_{28.1}Sb_{6.3}Se_{65.6}$ and $Ge_{12.5}Sb_{25}Se_{62.5}$ thin films given in Table 1 can be attributed to measurement uncertainty (± 0.01). To conclude, parameters of fabricated MIR structure are in very good agreement with the simulation of optical waveguide.

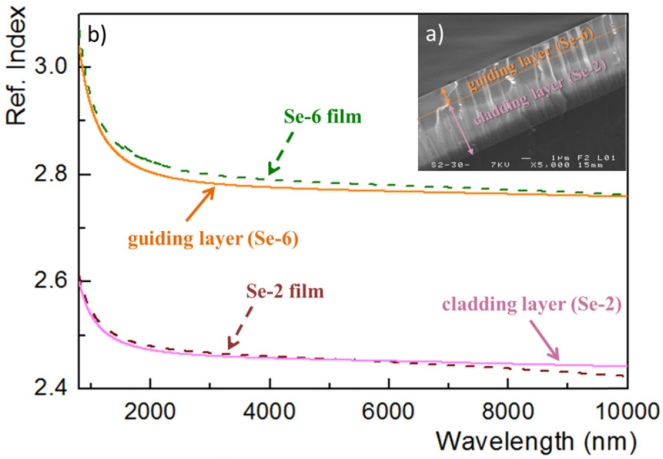

Fig. 5. (a) SEM image of MIR structure and Fig. 5(b) dispersion curves of refractive indices of $Ge_{28.1}Sb_{6.3}Se_{65.6}$, $Ge_{12.5}Sb_{25}Se_{62.5}$ single thin films, guiding and cladding layer of MIR structure estimated by the analysis of VASE data via Cody-Lorentz or Sellmeier model.

The ridge waveguide was obtained by using standard photolithography and RIE-ICP process. RIE-ICP allows samples etching with independently controllable flow and energy of ions bombarding over the substrate; this method was successfully used for chalcogenide thin films etching [47, 48]. The RIE/ICP power and the gas (CHF_3) flow were varied and optimized in order to obtain straight sidewalls with a low roughness and good delineation of the waveguides. To obtain ridge waveguide as illustrated in Fig. 6, the optimal parameters were RIE and ICP power of 25 and 75 W, respectively, and 5 sccm gas flow. The etch rate of selenide waveguides was about 400-500 $nm.min^{-1}$. Optical loss obtained in these ridge waveguides at 1.55 µm is ~0.7 ± 0.3 $dB.cm^{-1}$. This low value is in agreement with those obtained for chalcogenide planar waveguide [40] and chalcogenide ridge waveguides [8, 40, 49, 50]. The measurements performed by cut-back technique at 7.7 µm are in progress.

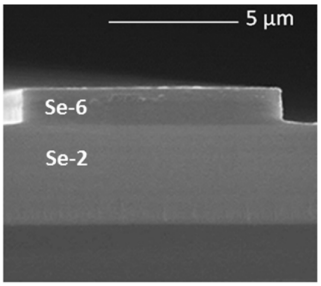

Fig. 6. SEM image of selenide ridge waveguide ($Ge_{12.5}Sb_{25}Se_{62.5}$ (Se-6) guiding layer and $Ge_{28.1}Sb_{6.3}Se_{65.6}$ (Se-2) cladding layer) fabricated by RIE-ICP using CHF_3 gas.

Optical Materials EXPRESS

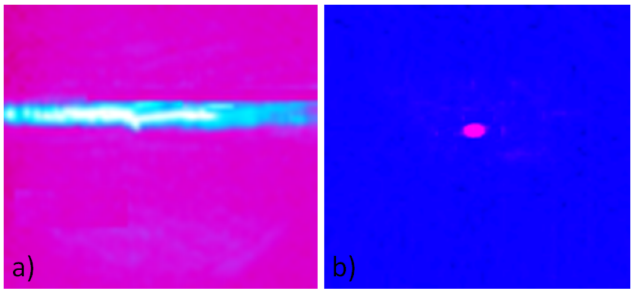

Fig. 7. (a) Near-field images in MIR (7.7 µm) representing the mode profile at the output of the planar waveguide and Fig. 7(b) the mode profile of single-mode ridge waveguide with 15 µm width.

In order to check the injection efficiency, the 1.55 µm light was coupled into the waveguide by a silica fiber. Once NIR characterization carried out at 1.55 µm, optical waveguides were characterized on a mid-IR optical bench at 7.7 µm using a chalcogenide fiber ($Ge_{10}As_{22}Se_{68}$). In this way, light injection was successfully conducted in MIR at 7.7 µm in planar (Fig. 7(a)) and ridge waveguides with widths ranging from 100 to 15 µm (Fig. 7(b)). We note a good confinement of the light in both, planar and ridge waveguides.

3.5. Functionalization of optical waveguide

Light propagation in the selenide waveguide has been demonstrated in MIR at 7.7 µm; nevertheless, due to strong absorbance and interference of water the detection of organic molecules in water requires hydrophobic material coating onto the surface of the waveguide [51]. In fact, functionalization of waveguide surface allows extraction of the analyte molecules from the solution so that they are detectable by the evanescent field. Polymers appear to be the most promising for this application; for example, polyisobutylene was already used for hydrocarbons detection [34]. Figure 8 presents SEM image of the functionalization of the optical waveguide by depositing PIB layer using spin coating method. An intimate contact between PIB and the selenide waveguide was clearly observed. Furthermore, polymer layer thickness of ~3.5 µm was obtained which corresponds to three times the penetration depth (Eq. (1), that can provide detection limits of pollutants molecules in the ppb range using mid-infrared evanescent field spectroscopy [45, 52]. The fundamental limit of detection for Ge-Sb-Se sputtered waveguides without polymer coating is typically a few tens of ppm.

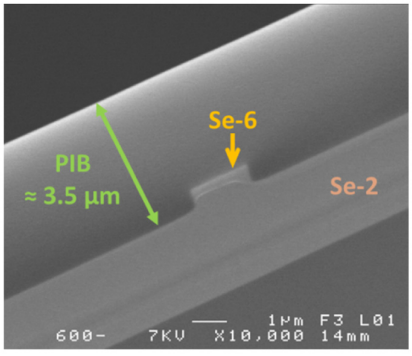

Fig. 8. SEM image of polyisobutylene film deposited on chalcogenide waveguide constituted of $Ge_{12.5}Sb_{25}Se_{62.5}$ (Se-6) guiding layer and $Ge_{28.1}Sb_{6.3}Se_{65.6}$ (Se-2) cladding layer.

4. Conclusions

In conclusion, we have successfully designed, fabricated and characterized evanescent field waveguide based on a cladding $Ge_{28.1}Sb_{6.3}Se_{65.6}$ layer and a guiding $Ge_{12.5}Sb_{25}Se_{62.5}$

Optical Materials EXPRESS

layer exploiting RF magnetron sputtering and RIE-ICP dry etching process. It is necessary to highlight that with respect to current literature, the use of tailored chalcogenide films compositions from Ge-Sb-Se system brings new opportunities not only regarding the variable refractive index contrast between individual layers of photonics structures but also avoids the use of arsenic-containing materials, which seem to be environmentally unacceptable. Waveguide was studied by NIR and MIR ellipsometry in order to study refractive index and thicknesses of each layer. Planar waveguide losses were measured to be ~0.7 $dB.cm^{-1}$ at 1.55 µm. Then, the light injection efficiency experiments were carried out in NIR (1.55 µm) and MIR (7.7 µm) in planar and ridge waveguides; the light confinement was observed for both designs. Finally, to detect pollutant molecules in water by the evanescent field, the waveguide surface was functionalized by depositing a polymer film by spin coating. As a result, we demonstrated the feasibility of chalcogenide waveguides fabrication for MIR detection of organic molecules in water. The experiments confirming the detection of molecules absorbing in MIR using fabricated waveguides are under progress and will be published separately.

Acknowledgments

Authors are thankful to Region Bretagne, IFREMER, BRGM, ANR LOUISE, Czech Science Foundation (Project No. 16-17921S) and CONACYT for PhD funding.